A hygrothermal modelling approach to water vapour sorption isotherm design for mesoporous humidity buffers

Fernando Sarce Thomann [a*], Matthew R Hall [a], Wantana Sangchoom [b] Robert Mokaya [b],

[a] *Division of Materials, Mechanics and Structures, Faculty of Engineering, University of Nottingham, University Park, Nottingham, NG7 2RD, UK*

[b] *School of Chemistry, Faculty of Science, University of Nottingham, University Park, Nottingham, NG7 2RD, UK*

*corresponding author - Email: emxfs@nottingham.ac.uk; Tel: +44 (0)115 8467873

Abstract

This paper describes the development of a design technique using hygrothermal numerical modelling for top-down predictive design and optimisation of water vapour sorption isotherms to match any humidity buffering application. This was used to inform the design and synthesis of two new mesoporous silica (MS) materials suitable for specific applications. To validate the technique, the new materials were experimentally assessed using gravimetric dynamic vapour sorption (DVS). The experimental isotherms closely matched the optimised isotherm predictions from the design stage, and a positive correlation was observed between the rate of change in adsorbed water content, Δw and the time taken to exceed the permissible upper limit of humidity, $\varphi_{i,U}$ in a closed environment. A positive non-linear correlation was determined between the interior volumetric moisture load, ω_{ml} and the mass of adsorbent required to fully achieve humidity buffering between specified lower/ upper limits ($\varphi_{i,L}$ and $\varphi_{i,U}$). The kinetics of water vapour sorption/ desorption were found to have general agreement when using the current hygrothermal numerical model. Current hygrothermal models appear to significantly underestimate the rate of adsorption/ desorption in rapid-response mesoporous

silica type materials. This is perhaps largely due to the current lack of consideration for scanning curve prediction within hysteresis loops and so is a priority for future research.

Keywords: hygrothermal modelling; water vapour isotherm; isotherm design; humidity buffering

Nomenclature

$\boldsymbol{\rho}$	Bulk density	kg/m³
$\boldsymbol{c_p}$	Specific heat capacity	J/(kg K)
$\boldsymbol{\lambda(w)}$	Moisture-dependent thermal conductivity	W/(m K)
$\boldsymbol{\varphi}$	Relative vapour pressure (p_v/p_{sat})	-
$\boldsymbol{n}$	Bulk porosity	m³/m³
$\boldsymbol{w = f(\varphi)}$	Water vapour sorption isotherm	kg/m³
$\boldsymbol{\mu(\varphi)}$	Water vapour diffusion factor	-
$\boldsymbol{D_w(w)}$	Liquid water diffusivity	m²/s
RH	Relative humidity; where $\varphi \cdot 100$	%
$\boldsymbol{\omega_{ml}}$	Volumetric moisture load	g/h/m^3
H	Total enthalpy	J/m^3
h_v	Latent heat of phase change	J/kg
t	Time	s
T	Temperature	K
δ_p	Vapour permeability	kg/(msPa)

Suffixes:

i	interior
e	exterior
L	lower limit
U	upper limit

1. Introduction

Regulation of the psychrometric variables within pre-defined upper/ lower limits, to match the requirements of 'closed environments' (*e.g.* cars, aircraft, buildings, incubators, laboratories, archives, *etc.*) accounts for the vast majority of global energy consumption and all associated emissions [1-3]. The study of hygrothermics considers an enclosed volume of air in which the psychrometric conditions are isolated from the exterior environment by limiting the exchange of heat, air, and moisture. In relative humidity (RH) buffering applications desirable hygrothermal behaviour is a material's capacity for simultaneous buffering of fluctuations in energy (air enthalpy) and mass (water vapour) concentration with respect to equilibrium moisture content [4, 5]. Some examples of moisture buffering applications in closed environments are preventing mould formation [6-9], building fabric damage [10-12], regulating thermal comfort for human activities [13-17], and energy efficient retrofit of existing/ older buildings [18-20]. On the other hand, disregarding RH buffering from hygrothermal materials lead to energy and cost penalties. These are caused by relying on continuous use of air conditioning (normally oversized) regardless of occupation, reducing the efficiency of the systems and increasing the energy consumption [21-23]. Advanced mesoporous materials could be then used to fully buffer fluctuations in psychrometric variables by designing them to have hygrothermal properties compatible with the pre-defined upper/ lower limits of any closed environment.

Hygrothermics studies the coupled phenomena in porous solids that occur as a result of adsorption, diffusion, and desorption of heat and moisture (liquid and vapour phases). The moisture storage function is one of several hygrothermal functional properties, where $w = f(\varphi)$ defines the non-linear relationship between the mass of adsorbed water and the ratio of vapour pressure to saturation vapour pressure; known as a sorption isotherm when at constant temperature. The maximum value for w depends on n, corresponding to total pore volume,

whilst $\lambda(w)$ describes the positive dependency of thermal conductivity on w. The summation of c_p for the adsorbent and adsorbate describe stored energy, whilst substantial heat transfer can occur due to both heat of adsorption and evaporation/ condensation of the adsorbate during transport. In the hygroscopic domain, the (Fickian) diffusion coefficient is a function of relative vapour pressure, $\mu(\varphi)$ as a result of pore network constriction by condensation filling. In the capillary domain, the water diffusion coefficient is a function of water content, $D_w(w)$ [24, 25]. This leads to the well-known contra- and counter flow mass transport scenarios in hygrothermics (see Fig. 1) [26, 27].

The morphology and volume of the pore network in mesoporous silicas can be easily modulated through the synthesis process (using surfactants as a template for polycondensation of silica species) by controlling the temperature [28, 29] and reaction time [30, 31]. This makes them an ideal template material from which to control and synthesise hygrothermal functional properties with respect to RH buffering. Significant interest in these materials has previously focussed on catalysis [32-34], separation [35-37], gas adsorption [38-40], and drug delivery [41, 42]. However, hygrothermics not only has to consider isothermal physisorption but also the temperature-dependency of heat & moisture diffusion and storage, as well as the moisture-dependency of thermal conductivity and heat storage. Hygrothermal models are constitutive and so require bulk-scale functional properties as inputs to represent mesoporous solids. The bulk-scale properties are therefore statistically-averaged representations of the mesopore-scale behaviour. In recent work, two important principles were established for the hygrothermal behaviour of mesoporous solids: (i) an empirical correlation between mesopore diameter and the kinetics of RH buffering [43], and (ii) prediction of the required adjustment to the hygrothermal functional properties of one mesoporous solid in order to duplicate the behaviour of another [20]. However, the relationships between structure (mesopore geometry,

physisorption and hysteresis) and properties (hygrothermal functions) are still neither quantified nor fundamentally understood.

The aim of this study was to develop a hygrothermal numerical modelling technique that enables top-down predictive design of the ideal water vapour sorption isotherm for any RH buffering application. The parameters for design would be a closed environment of volume, V in which the upper and lower limits for psychrometric variables (T_{max}, T_{min}, φ_{max}, φ_{min}) were specified. This technique was developed using three pre-existing materials from a previous study, and then used to inform the synthesis of two new MS; both having hygrothermal properties optimised to suit two different closed environment scenarios. The water vapour sorption isotherms and RH buffering behaviour of these two materials were then assessed experimentally.

2. Experimental

2.1. Synthesis and characterization

The two new pure silica MCM-41 samples were synthesized from fumed silica as silica source, cetyltrimethylammonium bromide (CTAB) as structure directing agent or template, tetramethylammonium hydroxide (TMAOH) and water. In a typical synthesis, 1.9 g TMAOH and 4.6 g CTAB were dissolved in 34.1 g of distilled water under stirring at 35 °C, following which 3.0 g fumed silica was added to the solution under stirring for 1 h to obtain a homogeneous gel of molar composition SiO_2:0.25CTAB:0.2TMAOH:40H_2O, which was left to age for 20 h at room temperature. The aged gel mixtures were then transferred into a Teflon-lined autoclave and heated, under static conditions, at 150 or 180 °C, for 48 h. The solid product was then filtered off, washed with water and dried in air at room temperature to yield the as-synthesized sample. The surfactant templates within the as-synthesised sample were removed by calcination (heating ramp rate of 5 °C/min) at 550 °C for 6 h. The final

calcined silica samples were designated as MCM-41-x where x is the synthesis (crystallisation) temperature, *i.e.*, 150 or 180 °C.

2.2. Material Characterisation

Powder X-ray diffraction (XRD) analysis was performed using a PANalytical X'Pert PRO diffractometer with Cu-Kα radiation (40 kV, 40 mA), 0.02 step size and 50 s step time. Nitrogen sorption isotherms and textural properties were determined at -196 °C using a conventional volumetric technique by a Micrometrics ASAP 2020 sorptometer. Before analysis, the samples were first dried at 130 °C and then outgassed under vacuum at 200 °C for 12 h. The surface area of the materials was determined using the standard Brunauer–Emmett–Teller (BET) method based on adsorption data in the relative pressure (P/P_o) range of 0.05 - 0.2, and pore volume was calculated from the amount of nitrogen adsorbed at P/P_o of ca. 0.99. Pore size distributions were obtained using density functional theory (DFT) analysis of adsorption data.

For enabling calibration of the hygrothermal modelling technique, three pre-existing mesoporous solids (MS 3.3, 4.7 and 8.3) of varying pore diameter and pore volume were taken from previous research [43] (see Table 1). Pore diameter was controlled during synthesis [43] by using alkyltrimethylammonium ($C_nH_{2n+1}(CH_3)_3N^+$ *n=16* and ($C_nH_{2n+1}(C_2H_5)_3N^+$, *n=12, 16* [44] with large head group surfactant [45]. Pore geometry and specific surface area were measured in the same study using the Barrett–Joyner–Halenda (BJH) and BET methods with N_2 physisorption, and validated against high resolution transmission electron microscopy (HRTEM) and small-angle X-ray diffraction (SAXRD). The hygrothermal functional properties were determined using modified transient plane source (MTPS), differential scanning calorimetry (DSC) and DVS techniques, the results of which are summarised in Table 1. For this study, the validity of Kelvin's equation

was therefore assumed, and the cumulative pore volume histogram obtained from the water isotherms found good agreement with the mean pore diameters determined using the BJH method [43].

2.3. Design of hygrothermal properties

Existing hygrothermal model packages include (but not limited to) WUFI, DELPHIN, HAM and MATCH [46] which have been validated against experimental data over the past 15+ years, and addressed as part of the Annex 41 project [47]. Physical models are often used to simulate bulk-scale hygrothermal behaviour and to validate numerical model predictions for heat and moisture transport/ storage [48, 49]. Currently, all hygrothermal numerical models must (as a minimum) accurately represent the following bulk-scale transport and storage phenomena [50]:

- heat storage in dry materials and any absorbed water
- heat transport by moisture-dependent thermal conduction
- latent heat transfer by vapour diffusion
- moisture storage by vapour sorption and capillary forces
- moisture transport by vapour diffusion
- moisture transport by liquid transport (surface diffusion and capillary flow)

The *Wärme und Feuchte Instationär* (WUFI) hygrothermal numerical model, WUFI+ v2.5.3 (Fraunhofer, Germany), was used for this study [51, 52]. The LHS of Eq. 1 represents the moisture storage function, which is proportional to the derivative of the water adsorption isotherm ($\partial w/\partial \varphi$). The transport terms on the RHS of Eq. 1 are described by the divergence of liquid and vapour flow. While vapour pressure ($p_v = \varphi \cdot p_{sat}$), which is the driving potential for vapour flux, is strongly temperature-dependent (saturation pressure $p_{sat} \sim \exp(T)$), liquid flow is governed by capillary forces which are assumed to be a function of RH only (*i.e.* from

Kelvin condensation). The LHS of Eq. 2 describes the enthalpy of air inside the closed environment, whilst the RHS describes heat transport due to solid conduction and diffusion of heat associated with the specific enthalpy of vapour water.

$$\text{Moisture balance: } \frac{dw}{d\varphi} \cdot \frac{\partial \varphi}{\partial t} = \nabla \cdot \left(D_w \nabla \varphi + \delta_p \nabla (\varphi \cdot p_{sat}) \right) \quad \text{Eq. 1}$$

$$\text{Energy balance: } \frac{dH}{dT} \cdot \frac{\partial T}{\partial t} = \nabla \cdot (\lambda \nabla T) + h_v \nabla \cdot \left(\delta_p \nabla (\varphi \cdot p_{sat}) \right) \quad \text{Eq. 2}$$

2.3.1 Approach to water isotherm design

For RH buffering applications it was hypothesised that the optimum isotherm would have the maximum theoretical pore volume and a steep w: p_v/p_0 gradient between the upper (φ_{max}) and lower (φ_{min}) limits of a given scenario. Following the same logic, this would imply that all candidate isotherms could be described by a transition from Type I to Type V (inclusive). For a closed environment with internal moisture sources (either fixed, intermittent or variable) the material will fail if the (user-defined) upper limit for indoor RH (φ_{max}) is exceeded. Conversely, if infiltration by exterior air (with much lower moisture content) occurs, the material will fail if the lower limit for indoor RH (φ_{min}) cannot be reached. An optimum sorption isotherm is therefore one that can maintain the fluctuation $\varphi(t)$ between the upper/ lower limits (φ_{max} and φ_{min}) of the given scenario. If after subsequent cycles the capacity for moisture storage decays, then after N cycles the fluctuation between φ_{max} and φ_{min} can no longer be maintained and the adsorbent must be fully outgassed for re-use. The initial approach was to (i) generate new isotherm candidates by modifying the isotherms of existing MS 3.3, 4.7 and 8.3 materials (see Section 2.3.3), (ii) conduct sensitivity analysis to correlate the effects of isotherm modification on RH buffering behaviour (see Section 3.1), and (iii) develop a refinement technique to produce an optimum isotherm for any closed environment scenario (see Section 3.2 to 3.4).

2.3.2 *Sensitivity analysis*

Sensitivity analysis was conducted by selecting the MS materials (MS 3.3, 4.7 and 8.3) from previous research [43]. The fluctuation of $\varphi(t)$ and the material's capacity for humidity buffering were assessed for a closed environment scenario in which the operating limits were φ_{max} = 0.70 and φ_{min} = 0.55, and the number of moisture loading cycles, N = 60. Each cycle comprised 2 h moisture generation (at a rate of 2.5 g/h) followed by 2 h of no moisture generation (4 h total). The closed environment comprised a thermally and hygrically isolated box (where V = 1 m^3) with an air infiltration rate of 0.35 ACH h^{-1}. The initial indoor/ outdoor air humidity (φ_i = 0.5, φ_e = 0.5 respectively) conditions were isothermal (T_{db} = 23°C). The fabric comprised 2 mm thick vapour barrier (S_d = 1500 m) and 240 mm thick vacuum insulation panel (λ = 0.001) (Fig. 2). A non-visualized internal component comprising 2 mm thickness of mesoporous solid (area/volume ratio = 0.12 m^2) was used and the hygrothermal functional properties taken from Table 1. The parameters for the numerical model were set to have: (i) increased accuracy and adapted convergence, (ii) net volume = 1 m^3, (iii) time step 1 min, (iv) optional climate (50% RH/ 23 °C), (v) inner climate calculated, (vi) initial boundary conditions (50% RH/ 23 °C), (vii) 'fine' mesh grid spacing, and (viii) calculation accuracy of 0.5% / 0.5°C for RH and T_{db} respectively.

2.3.3 *Candidate isotherms*

The first set of candidate isotherms were introduced (A_1 - A_6) and derived from MS 8.3, each having identical moisture storage capacity (identical Δw = 671 kg m^{-3}) within the specified $\varphi_{i,L}$ - $\varphi_{i,U}$ range, *i.e.* 0.45 - 055; 0.5 - 0.6; 0.55 - 0.65; 0.6 - 0.7; 0.65 - 0.75; 0.7 - 0.8 (Fig. 3a). Fig. 3b shows the modal pore diameters derived from Kelvin's equation ranging from 2.85 nm to 6.56 nm, hypothetically created by altering pore wall thickness such that pore volume remained unaltered (see Fig. 4b). The region of the isotherm between $\varphi_{i,L}$ (1st inflection point; the onset of multilayer physisorption) and $\varphi_{i,U}$ (2nd inflection point; the percolation threshold) corresponds to the available moisture storage capacity, Δw for RH buffering between upper/

lower limits (see Fig. 4a). A second set of isotherm candidates (B_1 - B_4) were introduced by proportionally reducing the total pore volume (y-axis adjustment) from 90% to 60%. The A_3 candidate isotherm was used as a reference and so the modal pore diameter remained constant (Fig. 5). The water absorption coefficient *A* derived from MS 8.3 was used for all candidates, and the capillary transport coefficients (D_{ws} and D_{ww}) for use in the hygrothermal numerical model were calculated after producing the water vapour isotherm [26].

2.3.4 Standardization and parametric studies

The next series of hygrothermal simulations aimed to determine the total permissible moisture load (g/h) per unit mass (kg) before RH buffering failure occurred. Candidate isotherm A_3, with an assumed area/volume ratio of 0.1200 (equivalent to 0.15 kg/m^3), was used as the reference (based on the previous simulations) and parametrically assessed against a set of eight new area/volume ratios: 0.0405, 0.0810, 0.1619, 0.2024, 0.2429, 0.2834, 0.3239, and 0.3643. This was done in order to set the standardization process of volumetric moisture loads (ω_{ml}) in 1m^3 at N = 60. Same parameters for the hygrothermal numerical modelling were set as described in Section 2.3.2. For ventilation sensitivity analysis, the simulations were expanded at three different ACH (0.25, 0.5 and 0.7 h^{-1}). The effect of φ_e in diluting/ intensifying the interior moisture load was simulated. For this the simulations were expanded by adding five new different φ_e values (φ_e = 0.2, 0.3, 0.4, 0.6 and 0.7). For both cases, the internal moisture loads in the hygrothermal numerical modelling were added progressively until material's failure was found; this set the curve of total moisture loads that a specific quantity of material can cope. The accuracy of the curve was within 3%, so the error bars would not be visible in some cases.

A representative selection of the ω_{ml} curves from previous parametric assessment (ACH = 0.25 h^{-1} and φ = 0.5; ACH = 0.7 h^{-1} and φ = 0.5; ACH = 0.35 h^{-1} and φ = 0.2; ACH = 0.35 h^{-1} and φ = 0.7) were used in order to predict the total permissible moisture loads for the rest of

the isotherm candidates designed (A_1, A_2, A_4, A_5, A_6, B_1, B_2, B_3, and B_4). Expanded hygrothermal simulations were done by selecting any x-axis and y-axis values (quantity of material and ω_{ml}, respectively) from the predicted curves (see Section 3.3) and setting them into the hygrothermal numerical modelling. The aim was to determine whether the fluctuation of $\varphi(t)$, and the material's capacity for RH buffering within the specified operating limits (φ_{max} = 0.70; φ_{min} = 0.55), could still be maintained.

2.3.5 Hygrothermal model validation

The water vapour isotherms for the two new materials were determined by gravimetric DVS. A DVS Advantage-2 series (Surface Measurements Systems Ltd., London, UK) with incorporated ultra-microbalance (1µg sensitivity) and fully automated weighing/ purging was used to independently control T_{db} and RH to an accuracy of ±0.5 K and ±1.5%, respectively (vapour pressure accuracy ±1.5% p/p_0). The data was recorded automatically in 1 min time-steps using Advantage Control Software (ACS). Previous to the test and taring of the ultra-microbalance, the chamber was left to fully equilibrate at 23 °C and at constant nitrogen flow (10 sccm) for 1 h to ensure stability for baseline measurements accuracy. All samples were outgassed under vacuum at 120 °C for 12 h. A pre-heating sequence was set in the ACS (heating ramp rate of 2 °C/ min, from 23 °C) at 150 °C for 1 h prior to testing, to ensure that w = 0. A counter weight in the reference pan was set to zero, and the dry samples (~ 0.02 g) were loaded to set the initial mass. A full cycle of 21 steps (sorption/ desorption) was programmed to increase with a targeted relative vapour pressure from φ = 0.05 to 1 (φ = 0.05 intervals) along with the change in mass step (0.001%/ min) until equilibrium moisture content (EMC) was reached. This was performed at T_{db} 23 °C and to a constant water vapour flow rate of 100 sccm (0.1 L/ min).

A set of three experiments of water vapour sorption/ desorption kinetics aimed to establish the accuracy of the numerical model were undertaken using the DVS Advantage-2 series. The

kinetics of the moisture uptake was meant to sequentially fluctuate between pre-defined RH limits (20 - 30%; 30 - 50%; and 50 -70%). Each cycle comprised 2hrs of moisture sorption (30 - 50% RH) followed by 2hrs of moisture desorption (50 - 30% RH) for a total period of 16 hrs (4 complete cycles). All samples were outgassed under vacuum at 120 °C for 12 h prior to testing. The same pre-heating sequence was applied using ACS, as previously described. Additionally, the samples were pre-conditioned within the DVS at constant mass to ensure that w_{20}, w_{30} and w_{50} were at EMC before the cycles started. The same steps for taring and equilibration of the chamber were done, and the samples (~ 0.02 g) were loaded to set the initial mass. This was again performed at T_{db} 23 °C and to a constant water vapour flow rate of 100 sccm (0.1 L/ min), as with previous experiments.

The hygrothermal numerical model setup was designed to sequentially perform the kinetics of the moisture uptake between the pre-defined RH limits (20 - 30%; 30 - 50%; and 50 - 70%) over a set number of cycles (as described previously – see Section 2.3.2 for description of the closed environment and the parameters of the numerical model). Scaling of the volume from the DVS chamber (V_{ch} = 0.0002945 m^3) to the physical model (V = 1 m^3) was done in order to proportionally set the infiltration rate of 100 sccm (0.006 m^3 h^{-1}) and the material quantity (0.02 g). As a result, a constant ACH = 20.37 h^{-1} and area/ volume ratio (0.01) of the non-visualized component was estimated. The initial w was set according to each test (EMC at w_{20}, w_{30} and w_{50}) intended to perform each sorption/ desorption cycle at constant temperature, where T_{db} = 23 °C.

3. Results and discussion

3.1. Sensitivity analysis of candidate isotherms

Fig. 6 shows the simulated RH buffering results for MS 3.3, 4.7 and 8.3 over the 4-hour cycle. Repeated long-term loop cycling of the material resulted in progressive decay of their

capacity for humidity buffering in cases where the moisture load was always positive, *i.e.* where no infiltration of lower moisture content air occurs. This decay caused the material to fail after N number of cycles when the fluctuation of $\varphi(t)$ exceeded the $\varphi_{i,U}$ limit. There appears to be no dependent correlation between N and modal pore diameter, where for MS 8.3, N = 6.5; MS 4.7, N = 3.5; and MS 3.3 N = 8.5. It was found that the number of decay cycles, N, was highly sensitive to the value of Δw between $\varphi_{i,L}$ - $\varphi_{i,U}$ limits, *i.e.* controlled by φ (x-axis) adjustments to the sorption isotherm and hence pore size distribution. From Fig. 7a it appears that the largest proportion of water uptake (candidate isotherm A_3) corresponds to the longest time for material failure. Furthermore, Fig. 7b shows a positive linear correlation between the moisture storage capacity in the operating range of the isotherm ($\varphi_{i,L}$ - $\varphi_{i,U}$), in this case $\Delta w_{55\text{-}65}$, and the time taken to exceed the $\varphi_{i,U}$ limit. Fig. 7b shows that this linear correlation persists for B_1 - B_4, where reduction in pore volume gives a proportional increase in elapsed time before buffering failure (or N cycles). The slope of $\Delta w/ t$ linear correlation approximates that for other candidate isotherms that have been designed for different $\varphi_{i,U}$ and $\varphi_{i,L}$ limits (Fig. 8a- c).

3.2. Closed environment parameters

Fig. 9a-b shows the simulated results where a non-linear positive correlation was found between the interior moisture load per unit volume inside the closed environment, and the minimum quantity (mass) of adsorbent required to achieve buffering between $\varphi_{i,L}$ and $\varphi_{i,U}$. As the background air infiltration to the closed environment (ACH $^{-1}$) increased, the moisture content of the infiltrating (exterior) air either adds to or subtracts from the interior moisture load (g/s) and so the minimum mass of adsorbent required can be adjusted in accordance with the trends shown in Fig. 9a-b. If $\varphi_{i,L} \leq \varphi_e \leq \varphi_{i,U}$, then the RH buffering capacity of the adsorbent, and the surface area: volume ratio of adsorbent required becomes sensitive to ACH $^{-1}$. If $\varphi_e < \varphi_{i,L}$, the surface area: volume ratio of adsorbent reduces whilst N increases, and the

interior moisture loads can potentially be wholly offset by infiltration alone. Conversely, if $\varphi_e > \varphi_{i,U}$, N decreases and the adsorbent may not be able to buffer the closed environment unless ACH $^{-1}$ is very low.

3.3. Moisture loads prediction

As the number of decay cycles N is highly sensitive to Δw, the permissible moisture loads before failure (in this case at $N = 60$) could confidently be estimated for any candidate isotherm and any closed environment scenario. Fig. 10 shows the dependency of Δw on the added/ subtracted moisture load from infiltrating air (including infiltration rate) at different outdoor air humidities, φ_e. Expanded numerical simulations showed good agreement where the $\varphi_{i,L}$ - $\varphi_{i,U}$ limits were not exceeded at $N = 60$. This hygrothermal numerical modelling technique can therefore be applied to generate ω_{ml}/ adsorbent mass graphs for any closed environment scenario, from which the optimum surface area: volume ratio and air infiltration rate can be selected.

3.4. Experimental work and model validation

Fig. 11 shows the water vapour isotherm (sorption/ desorption cycles) for the two new materials (MCM-41$_{150}$/ MCM-41$_{180}$); both, having a distinctive Type V isotherm and type H2 hysteresis loop. From Fig. 11 it appears that there is a close fit between the ideal designed isotherms (MS-5.38 and MS-8.24) and the experimentally achieved ones, indicating a good correlation between their modal pore diameter and total pore volume. This was found to be 56% and 42% from the total pore volume (MS-5.38 and MS-8.24) for the cases of MCM-41$_{150}$ and MCM-41$_{180}$, respectively. This indicates that for MCM-41$_{180}$ the difference in total pore volume and modal pore diameter can be tuned by varying pore wall thickness during (crystallisation) synthesis by controlled temperature variation.

365 The moisture content between $\varphi = 0.65$ and 0.80 was found to be $\Delta w_{65\text{-}80} = 407.5$ kg m^{-3} for
366 MCM-41$_{150}$, $\Delta w_{65\text{-}80} = 256.4$ kg m^{-3} for MCM-41$_{180}$. Whereas between $\varphi = 0.70$ and 0.85, this
367 was found to be $\Delta w_{70\text{-}85} = 267.7$ kg m^{-3} and 307.0 kg m^{-3}, respectively. The numerical
368 simulations showed that the resultant progressive decay of their capacity was highly sensitive
369 according to their highest Δw values. Evidence of this is shown in Fig. 12 for the RH
370 buffering results where the number of decay cycles, N was ~ 1.7 times higher for MCM-41$_{150}$
371 compared to MCM-41$_{180}$. Here, the onset of multilayer physisorption (i.e. steep slope of Δw
372 gradient at $\varphi = 0.65$ - arrow seen in Fig. 11) is clearly higher for the MCM-41$_{150}$. This resulted
373 in lowering the fluctuation of $\varphi(t)$ below the $\varphi_{i,U}$ limit. Conversely, Fig. 13 shows a significant
374 increase in the number of decay cycles ($N = 12$) for MCM-41$_{180}$, which corresponds to a
375 higher $\Delta w_{70\text{-}85} = 39.3$ kg m^{-3} compared with MCM-41$_{150}$.
376
377 Fig. 14 shows the comparison between the experimental DVS and numerical simulations
378 results for the three water vapour sorption/ desorption kinetics experiments (A, B and C).
379 Experimentally, EMC was achieved within $N = 4$ with a distinctive steep sorption/ desorption
380 gradient (suggesting rapid response for moisture sorption/ desorption) for all cases except
381 MCM-41$_{150}$ operating at 50 - 70% RH. This could partially be an indication of pronounced
382 scanning curves within this region of the H2 hysteresis loop, and partially as a result of
383 having a higher Δw gradient ($\Delta w_{50\text{-}70} = 179.5$ Kg m^{-3}) compared with MCM-41$_{180}$ (see Fig. 11
384 and Fig. 14c). With the exception of MCM-41$_{180}$, operating in the 20 - 30% and 30 - 50% RH
385 ranges (full sorption/ desorption reversibility), it was found that the numerical predictions for
386 both the moisture uptake capacity and the rate of sorption (kinetics) were typically
387 underestimated. This could be attributable to the current absence of hysteresis loop and
388 associated scanning curve predictions within state-of-the-art hygrothermal simulation
389 techniques, and so clearly highlights this as a priority for future research.
390

4. Conclusions

A top-down predictive design tool that enables the design of an ideal water vapour sorption isotherm for any RH buffering application was developed and experimentally tested. The simulated results of this technique probed MCM-41 type materials and found that they can provide a wide range of suitable candidates for synthesizing/ modulating mesopore geometry and to enable optimisation of hygrothermal functional properties with respect to RH buffering. Evidence of this was found in the close fitting between experimental and designed isotherms and within a range that can be accurately matched or predicted by the design tool. Consistent agreement was found when correlating pore volume with pore wall thickness variance from the synthesis process, indicating a positive correlation between their Δw and the time in time in exceeding $\varphi_{i,U}$.

The simulated results showed that for any RH buffering application, the progressive decay for humidity buffering was independent of modal pore diameter and had a positive correlation with Δw between the $\varphi_{i,L}$ - $\varphi_{i,U}$ limits. Evidence of this was found in a positive linear trend between Δw and the time taken to exceed $\varphi_{i,U}$. This suggested that when designing an ideal isotherm for a specific application, adjustment of the maximum Δw should be allocated between the operating limits $\varphi_{i,L}$ - $\varphi_{i,U}$. A methodological illustration of the refinement technique logic for the design process of an ideal isotherm is presented in Fig. 15; a brief summary of steps (a) to (f) referred to it are as follows:

a) Preliminary assessment using the hygrothermal numerical model for any MS material (light blue line) under a specific buffering application, where fluctuation of $\varphi(t)$ is analysed within/ outside the $\varphi_{i,U}$ and $\varphi_{i,L}$ limits
b) Design a set of isotherm candidates from the MS material (light blue line), using its maximum w to set the maximum theoretical n possible
c) Corresponding PSD histogram derived from the isotherm candidates in (b)

d) Sensitivity analysis for all new candidates in (b) using the hygrothermal numerical model from (a). The aim is to find the most suitable water isotherm for the application

e) The ideal water isotherm is found (pink line) at a corresponding gradient between I_L and I_U, which steadily allowed for hygrothermal buffering at a higher number N of cycles from (d)

f) Further adjustment of the water isotherm related to φ (x-axis) and w (y-axis) adjustments, results in a variety of modal pore diameter and pore volume respectively for any kind of buffering applications

Expanded numerical simulations showed that for a closed environment, a positive non-linear correlation between the total permissible ω_{ml} and the mass of adsorbent required to fully achieve buffering between $\varphi_{i,L}$ and $\varphi_{i,U}$ was established. It was found that the RH buffering capacity and the volume ratio of the adsorbent were controlled by φ_e and ACH $^{-1}$; undermining/ improving the material's failure at N cycles. Furthermore, the permissible ω_{ml} changes proportionally with Δw from an ideal isotherm, and therefore could confidently be estimated for any candidate isotherm and any closed environment scenario. On the other hand, it was evident from the experimental results that the kinetics of the dynamic behaviour of water vapour sorption/ desorption (possible presence of scanning curves development within a specific hysteresis loop) is still not fully implemented by current hygrothermal numerical models. However, in this study some exceptions were found (MCM-41_{180} at the 20 - 30% and 30 - 50% RH limits), from which the concept of full sorption/ desorption reversibility enables hygrothermal structure-properties assessment.

5. Acknowledgements

The authors wish to gratefully acknowledge the support of CONICYT for funding this research through the 'Programa de Formación de Capital Humano Avanzado, BECAS

CHILE' – Ministerio de Educación, Gobierno de Chile. We also thank the Rajamangala University of Technology Srivijaya (RMUTSV), Thailand for funding and a studentship for WS.

6. References

[1] R.Z. Freire, G.H.C. Oliveira, N. Mendes, Energy and Build. 40 (2008) 1353-1365.

[2] L. Pérez-Lombard, J. Ortiz, C. Pout, Energy and Build. 40 (2008) 394-398.

[3] S.J. Davis, K. Caldeira, Proceedings of the National Academy of Sciences, 107 (2010) 5687-5692.

[4] M.R. Hall, Materials for energy efficiency and thermal comfort in buildings, CRC Press 2010.

[5] C. Hall, W.D. Hoff, Water transport in brick, stone, and concrete, Spon Press London 2012.

[6] G.H. dos Santos, N. Mendes, P.C. Philippi, International J. of Heat and Mass Transfer. 52 (2009) 4862-4872.

[7] V.M. Nik, A. Sasic Kalagasidis, E. Kjellström, Build. and Environ. 55 (2012) 96-109.

[8] K. Sedlbauer, J. of Build. Phys. 25 (2002) 321-336.

[9] M. Krus, K. Sedlbauer, Annex41 Report "A1-T4-D-5-1. pdf" in Trondheim Meeting, Trondheim, Norway 2005.

[10] M. Abuku, H. Janssen, S. Roels, Energy and Build. 41 (2009) 101-110.

[11] H.J. Steeman, M. Van Belleghem, A. Janssens, M. De Paepe, Build. and Environ. 44 (2009) 2176-2184.

[12] K. Sedlbauer, M. Krus, W. Zillig, H. Künzel, IAQ 2001: Moisture, Microbes, and Health Effects: Indoor Air Quality and Moisture in Buildings, (2001).

[13] M. Steeman, M. De Paepe, A. Janssens, Build. and Environ. 45 (2010) 1641-1652.

[14] O.F. Osanyintola, C.J. Simonson, Energy and Build. 38 (2006) 1270-1282.

[15] H.J. Steeman, A. Janssens, J. Carmeliet, M. De Paepe, Build. and Environ. 44 (2009) 572-583.

[16] M. Woloszyn, T. Kalamees, M. Olivier Abadie, M. Steeman, A. Sasic Kalagasidis, Build. and Environ. 44 (2009) 515-524.

[17] J. Laverge, N. Van Den Bossche, N. Heijmans, A. Janssens, Build. and Environ. 46 (2011) 1497-1503.

[18] S.P. Casey, M.R. Hall, S.C.E. Tsang, M.A. Khan, Build. and Environ. 60 (2013) 24-36.

[19] M.R. Hall, S.P. Casey, D.L. Loveday, M. Gillott, Build. and Environ. (2013).

[20] S.P. Casey, M.R. Hall, S.E. Tsang, M.A. Khan, J. of Build. Perform. Simul. 6 (2013) 354-366.

[21] R.M. Barbosa, N. Mendes, Energy and Build. 40 (2008) 276-288.

[22] A. Korjenic, T. Bednar, Appl. Therm. Engineering. 40 (2012) 275-283.

[23] M. Qin, G. Walton, R. Belarbi, F. Allard, Energy Convers. and Management. 52 (2011) 1470-1478.

[24] M. Hall, D. Allinson, Build. and Environ. 44 (2009) 1935-1942.

[25] H. Kuenzel, A. Karagiozis, A. Holm, A hygrothermal design tool for architects and engineers, ASTM International West Conshohocken, PA2001.

[26] H.M. Künzel, Simultaneous heat and moisture transport in building components, IRB-Verlag Stuttgart 1995.

[27] M. Krus, Moisture transport and storage coefficients of porous mineral building materials: Theoretical principles and new test methods, Fraunhofer IRB Verlag 1996.

[28] W. Sangchoom, R. Mokaya, J. of Mater. Chem. 22 (2012) 18872-18878.

[29] A. Corma, Q. Kan, M.T. Navarro, J. Pérez-Pariente, F. Rey, Chem. of Mater. 9 (1997) 2123-2126.

[30] A. Sayari, S. Hamoudi, Chem. of Mater. 13 (2001) 3151-3168.

[31] J. Lei, J. Fan, C. Yu, L. Zhang, S. Jiang, B. Tu, D. Zhao, Microporous and Mesoporous Mater. 73 (2004) 121-128.

[32] T. Maschmeyer, F. Rey, G. Sankar, J.M. Thomas, Nat. 378 (1995) 159-162.

[33] A. Corma, M. Navarro, J.P. Pariente, J. of the Chemical Society, Chemical Communications. (1994) 147-148.

[34] T. Blasco, A. Corma, M. Navarro, J.P. Pariente, J. of Catalysis. 156 (1995) 65-74.

[35] G.S. Attard, J.C. Glyde, C.G. Göltner, Nat. 378 (1995) 366-368.

[36] M.R. Jamali, Y. Assadi, F. Shemirani, M.R.M. Hosseini, R.R. Kozani, M. Masteri-Farahani, M. Salavati-Niasari, Analytica chimica acta. 579 (2006) 68-73.

[37] B.L. Newalkar, N.V. Choudary, P. Kumar, S. Komarneni, T.S. Bhat, Chem. of Mater. 14 (2002) 304-309.

[38] C. Knöfel, J. Descarpentries, A. Benzaouia, V. Zeleňák, S. Mornet, P. Llewellyn, V. Hornebecq, Microporous and Mesoporous Mater. 99 (2007) 79-85.

[39] G.P. Knowles, J.V. Graham, S.W. Delaney, A.L. Chaffee, Fuel Processing Technology. 86 (2005) 1435-1448.

509 [40] V. Zelenak, D.a. Halamova, L. Gaberova, E. Bloch, P. Llewellyn, Microporous and
510 Mesoporous Mater.116 (2008) 358-364.

511 [41] M. Vallet-Regi, A. Ramila, R. Del Real, J. Pérez-Pariente, Chem. of Mater. 13 (2001)
512 308-311.

513 [42] B. Munoz, A. Ramila, J. Perez-Pariente, I. Diaz, M. Vallet-Regi, Chem. of Mater. 15
514 (2003) 500-503.

515 [43] M.R. Hall, S.C.E. Tsang, S.P. Casey, M.A. Khan, H. Yang, Acta Materialia. 60 (2012)
516 89-101.

517 [44] A.M. Suman K J, and Seitaro N Catal. Surv. Asia. (2004) 1-13.

518 [45] J.F. Dongyuan Z, Qisheng H, Nicholas M, Glenn H F, Bradley F C, and Galen D S
519 Science. (1998) 548-552.

520 [46] J. Delgado, N.M. Ramos, E. Barreira, V. De Freitas, Journal of Porous Media. 13 (2010).

521 [47] M. Woloszyn, C. Rode, Building Simulation, Springer 2008, pp. 5-24.

522 [48] Z. Pavlík, R. Černý, Energy and Build. 40 (2008) 673-678.

523 [49] T. Kalamees, J. Vinha, Build. and Environ. 38 (2003) 689-697.

524 [50] B. Group, BS EN 15026 2007: Hygrothermal performance of building components and
525 building elements. Assessment of moisture transfer by numerical simulation, London, 2007.

526 [51] A. Karagiozis, WUFI-ORNL/IBP, Hygrothermal model, No. P01-111509. Oak Ridge
527 National Lab., TN (US), 2001.

528 [52] A. Karagiozis, H. Künzel, A. Holm, Performance of Exterior Envelopes of Whole
529 Buildings VIII, 2008, pp. 2-7.
530

7. List of figures

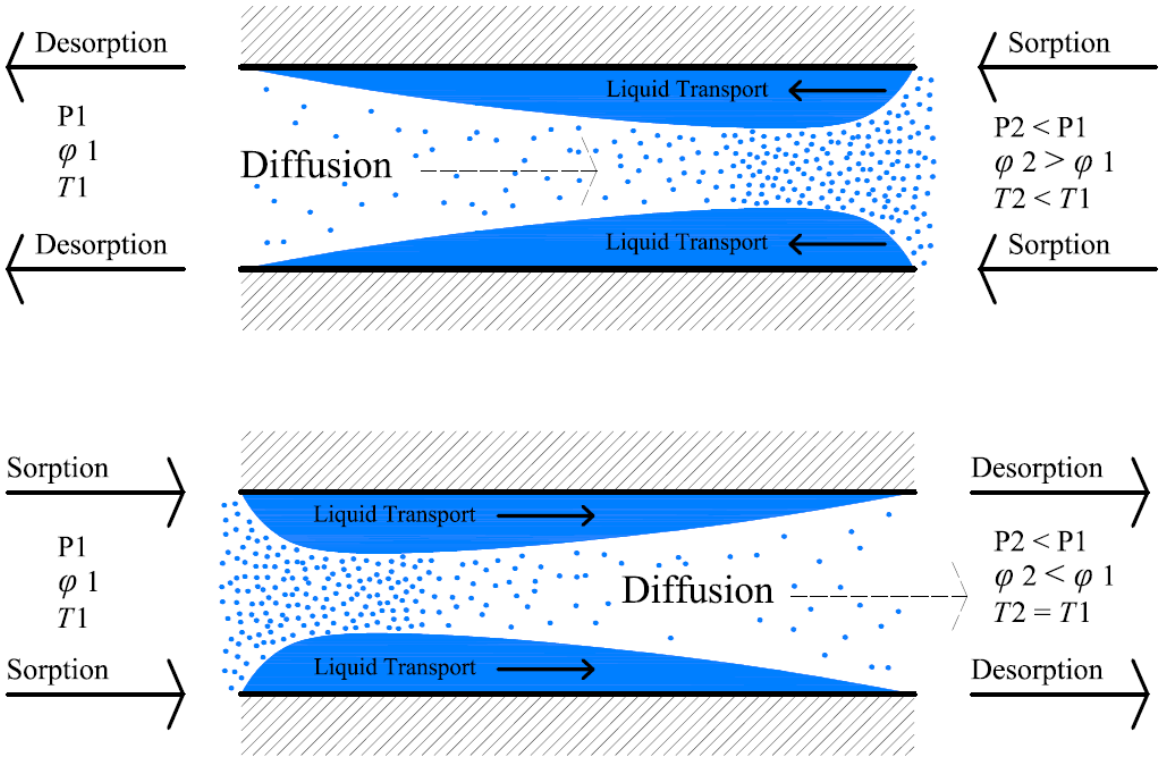

Figure 1 – Contra - and counter flow of mass transport. Adapted from [27]

548

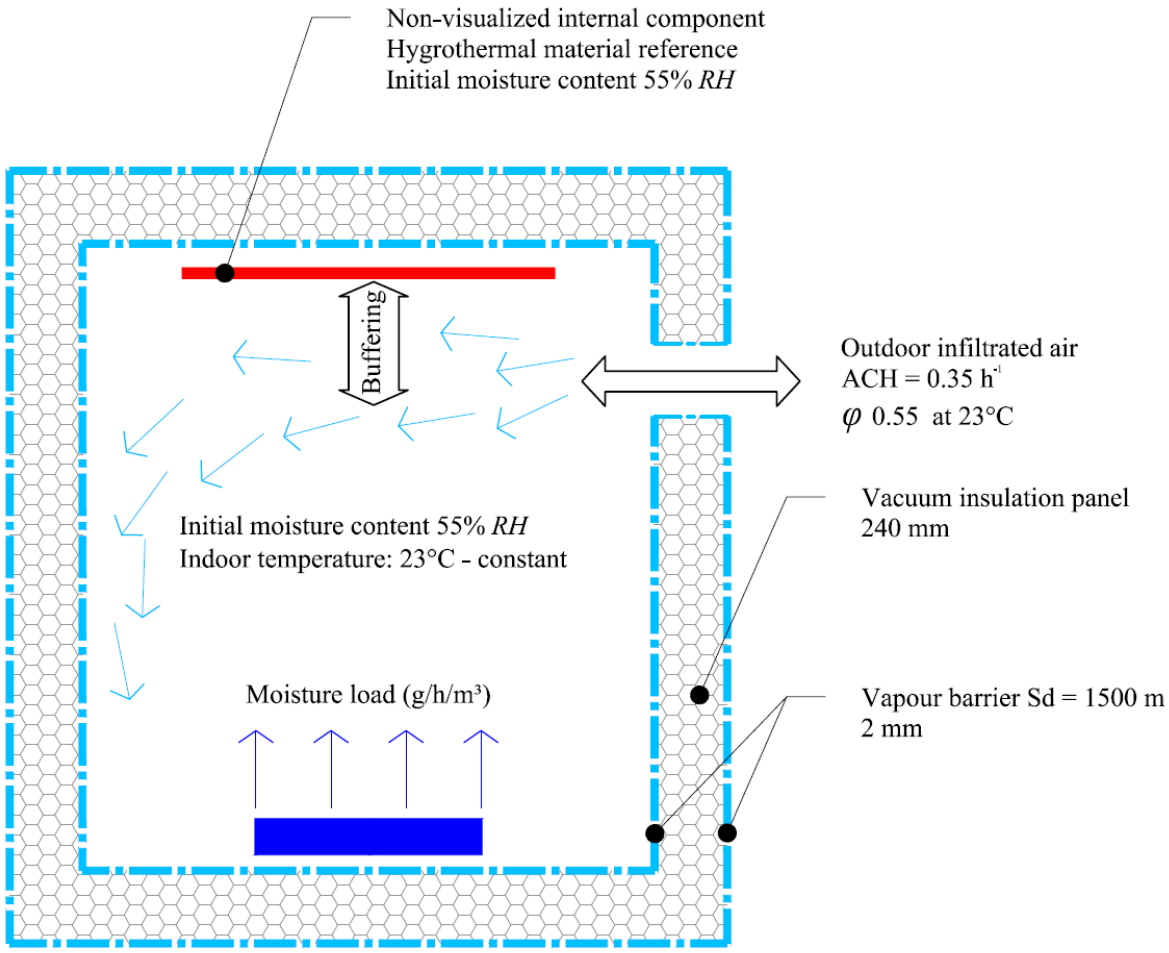

Figure 2 – Closed environment scheme

549

550

551

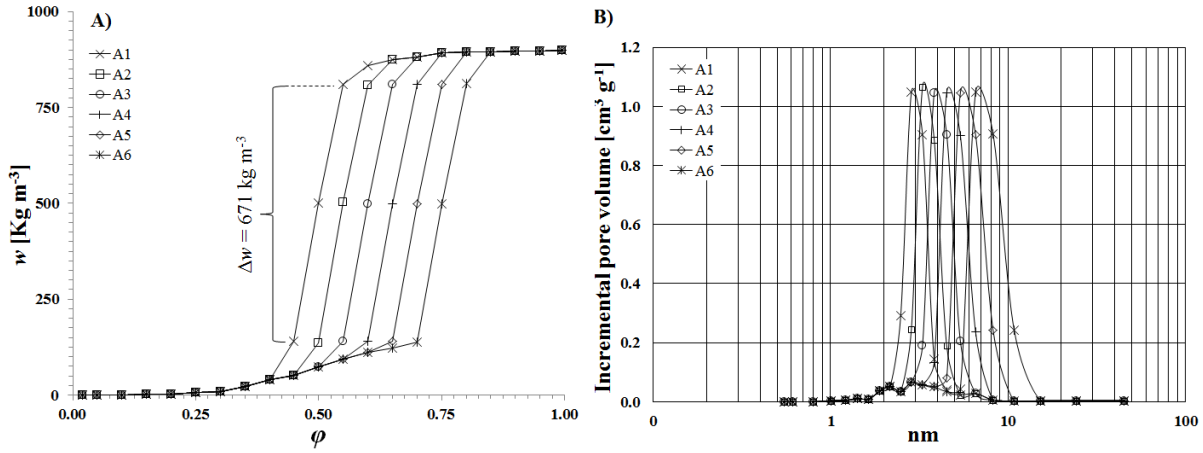

Figure 3 – Hypothetical water vapour isotherm, a) available moisture capacity Δ*w*, b) constant modal pore diameter and *n*

552

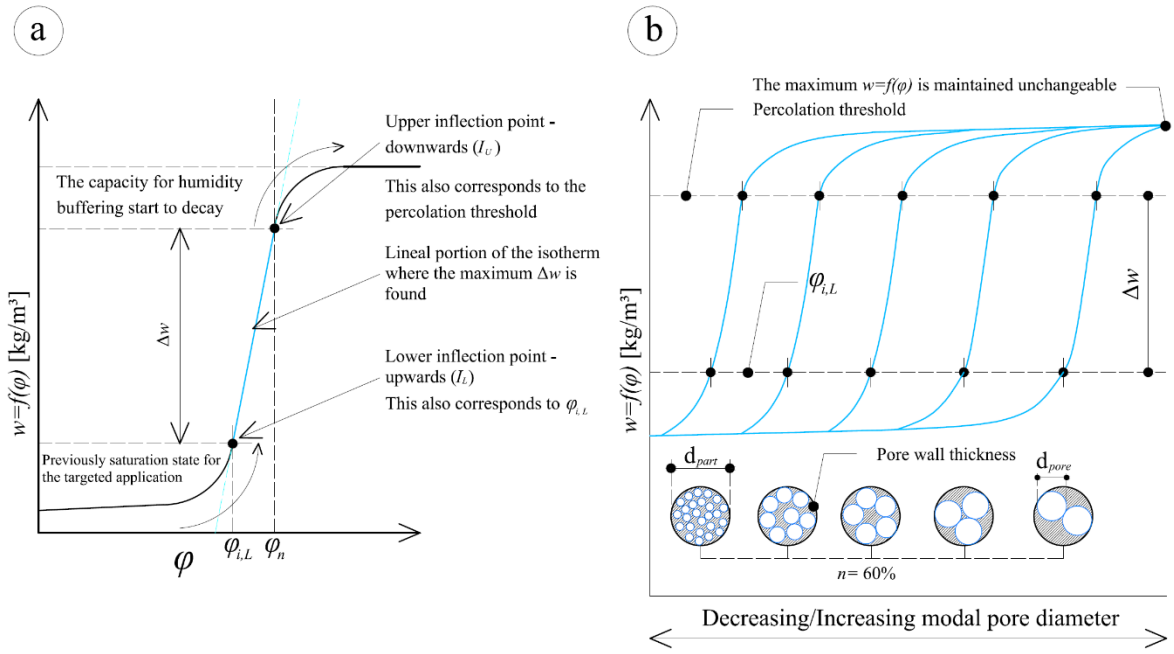

Figure 4 – RH buffering results for MS-3.3, 4.7 and 8.3

553
554

555

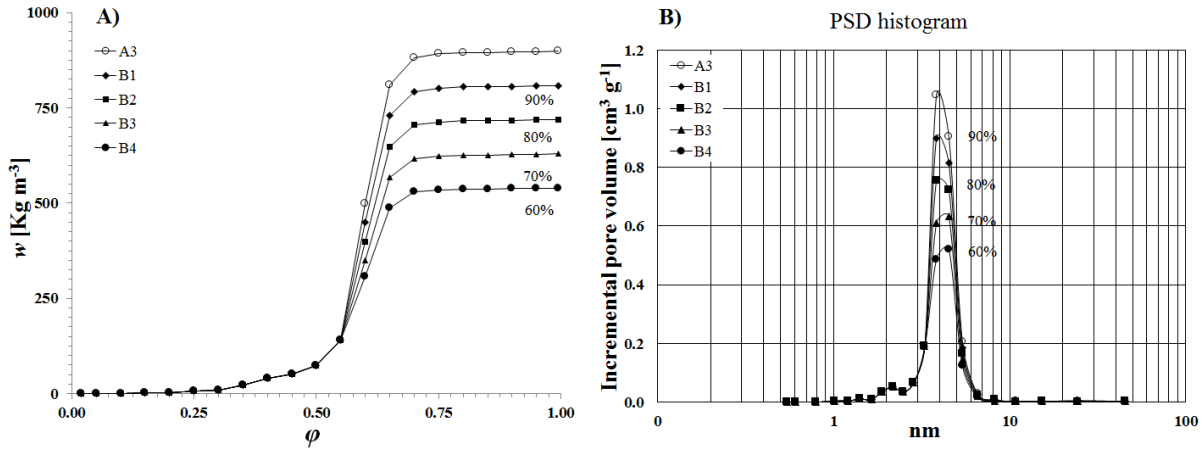

Figure 5 – Isotherm candidates, a) sorption isotherms, b) modal pore diameter derived from Kelvin's equation

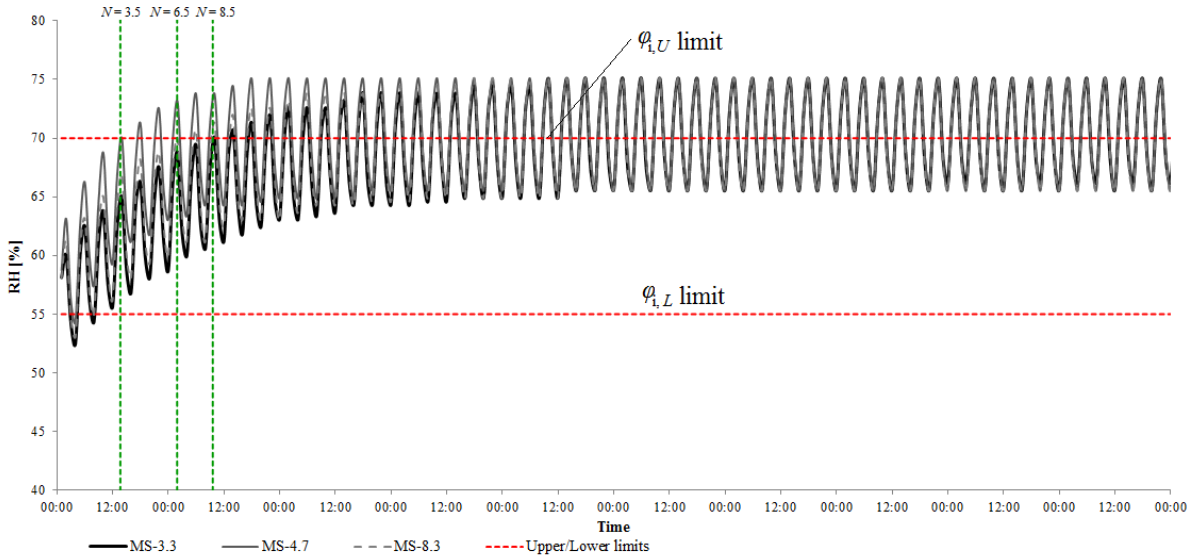

Figure 6 – Correlation between Δ*w* and moisture storage decay, a) water uptake at Δ*w* range, b) Δ*w*/ *t* linear correlation

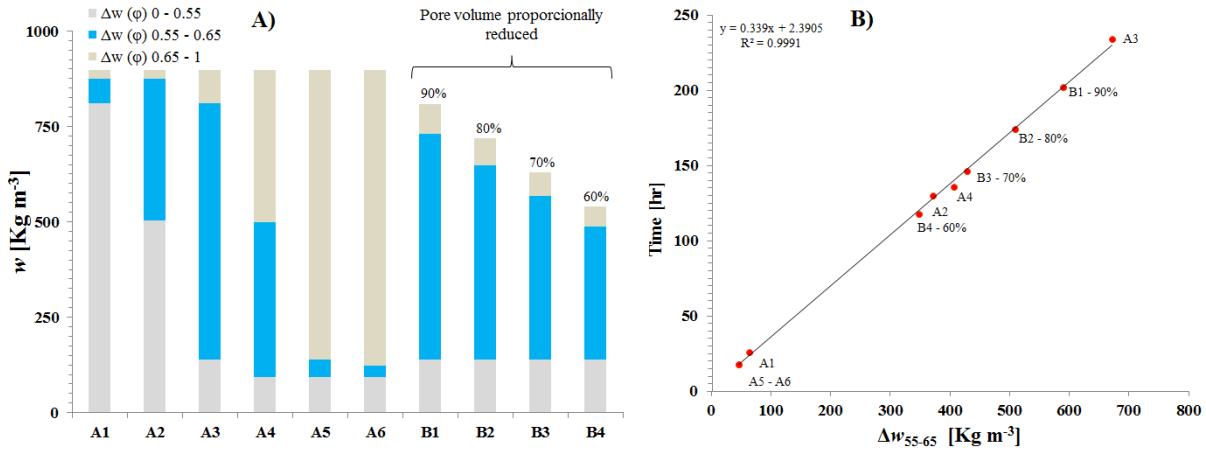

Figure 7 – Isotherm candidates – total pore volume proportionally reduced, a) sorption isotherms, b) modal pore diameter derived from Kelvin's equation

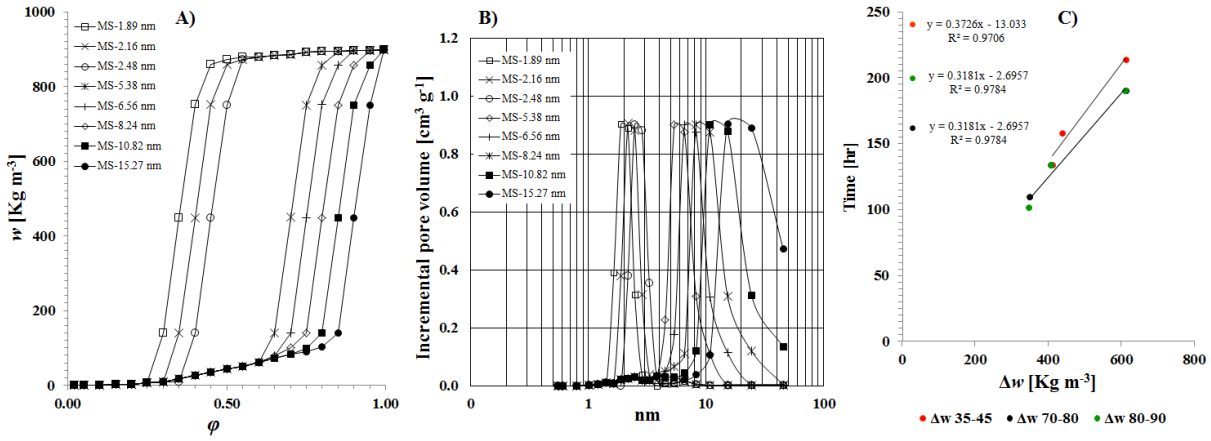

Figure 8 – Isotherm candidates for different $\varphi_{i,U}$ and $\varphi_{i,L}$ limits, a) sorption isotherms, b) modal pore diameter derived from Kelvin's equation, c) $\Delta w/\ t$ linear correlation

568

569

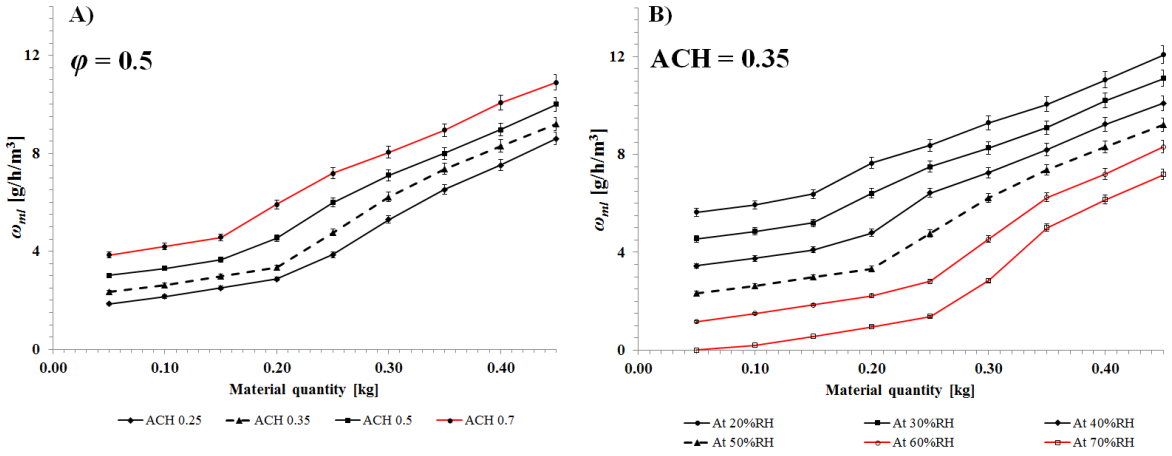

Figure 9 – Permissible volumetric moisture load curves, a) constant RH, b) varying ACH

570

571

572

573

574

575

576

577

578

579

580

581

582

583

584

585

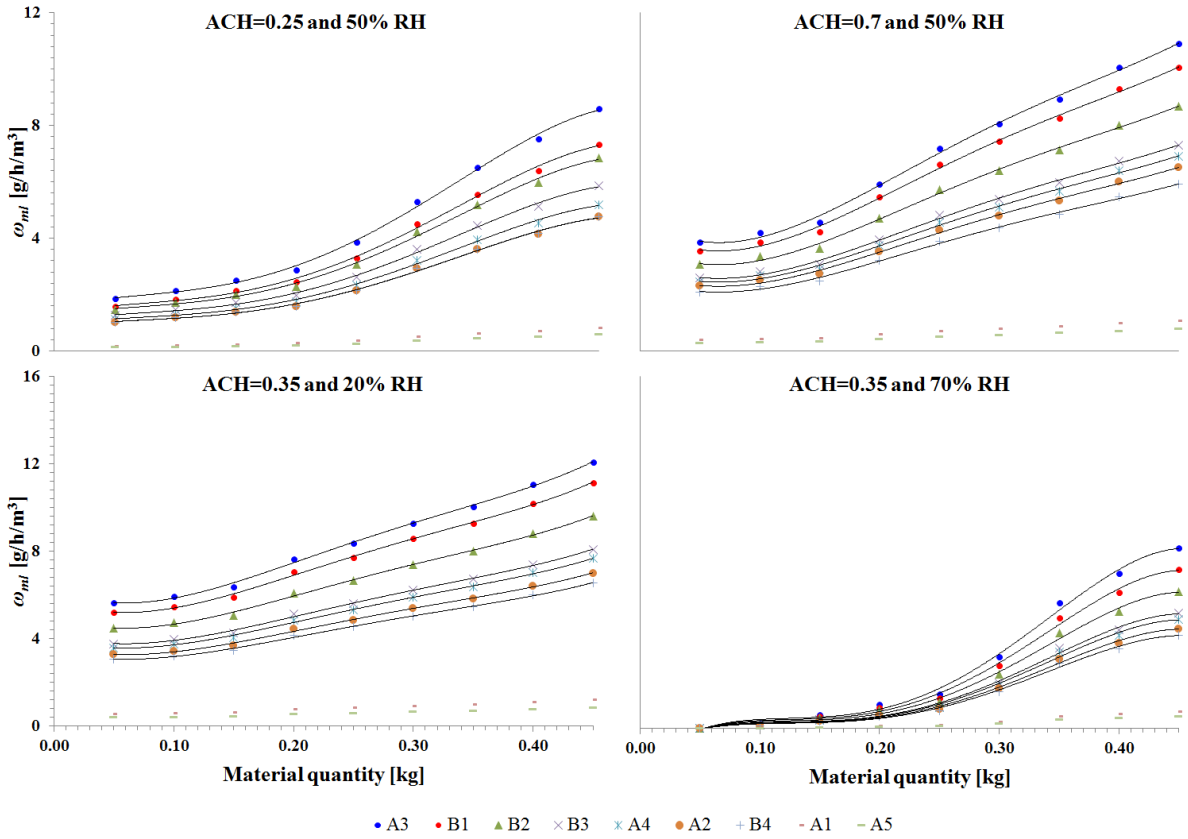

Figure 10 – Prediction of volumetric moisture load curves for designed isotherm candidates

586

587

588

589

590

591

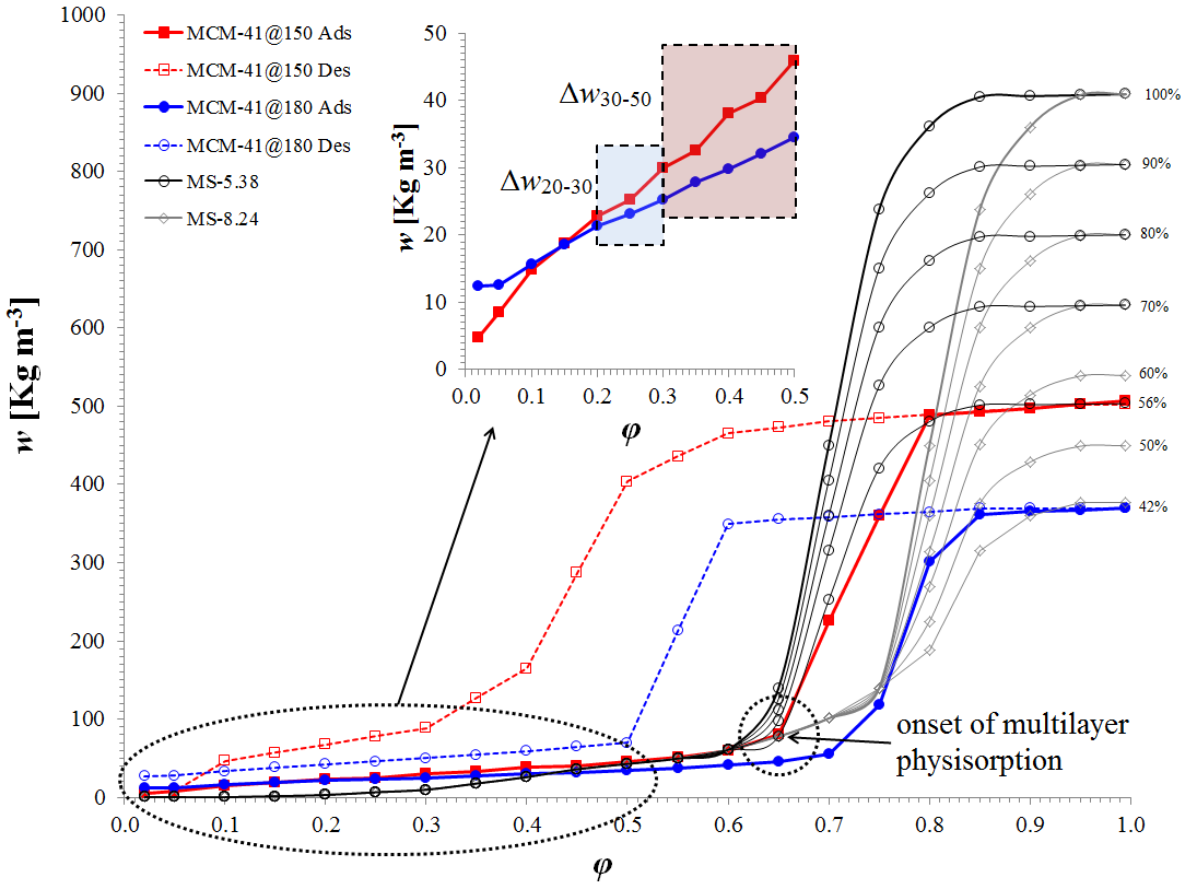

Figure 11 – Designed and experimental water vapour isotherms

592

593

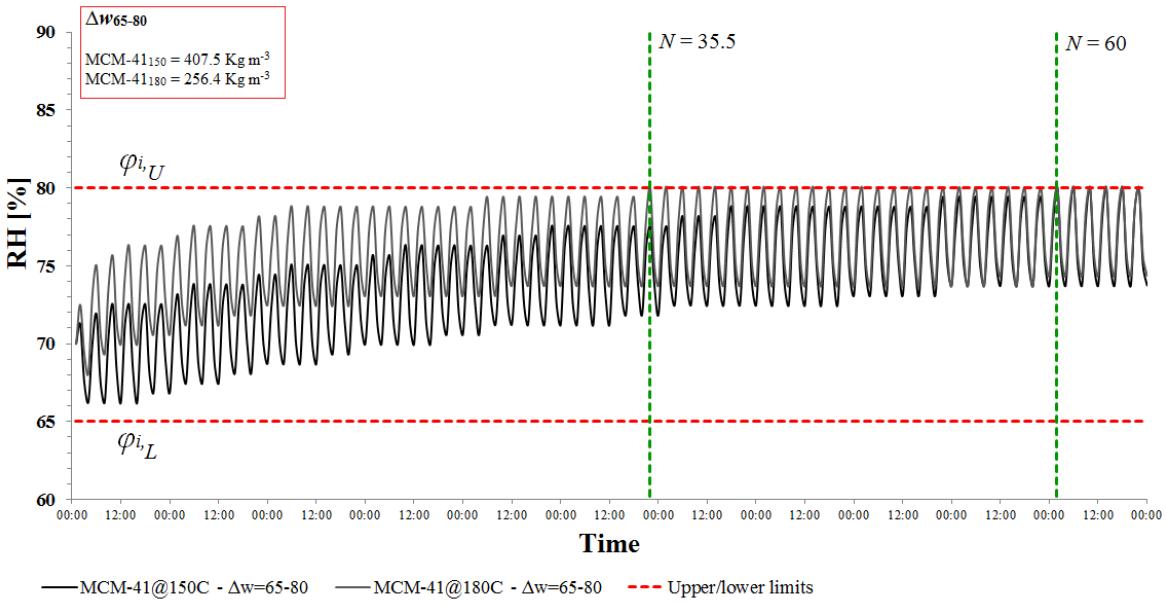

Figure 12 – RH buffering results for MCM-41$_{150}$ and MCM-41$_{180}$ – buffering application between $\varphi_{i,U}$ = 0.8 and $\varphi_{i,L}$ = 0.65

594

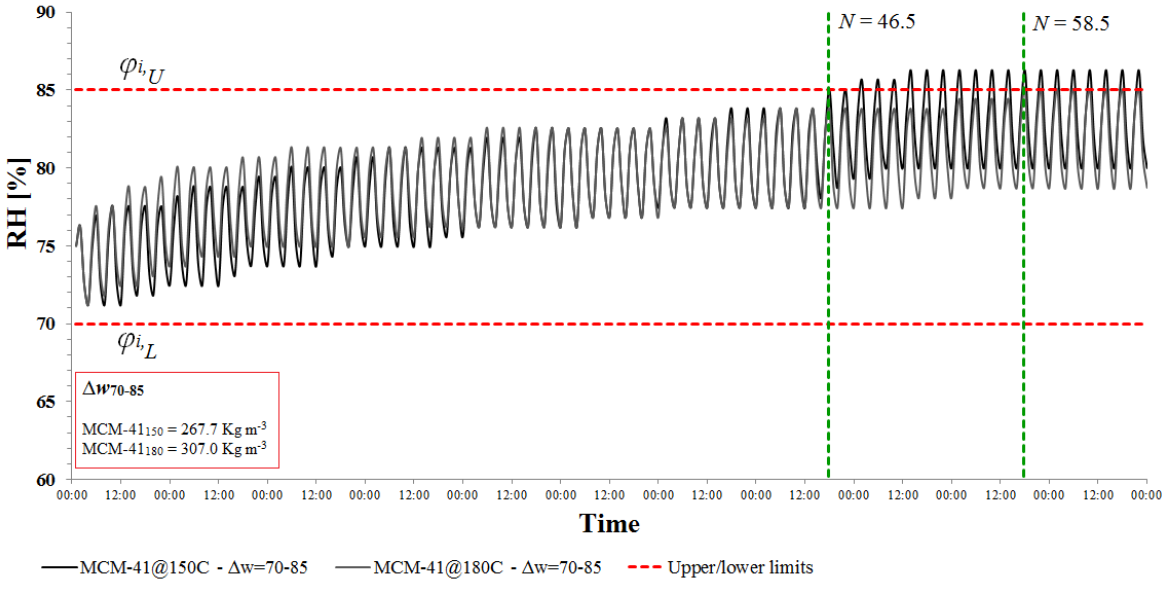

Figure 13 – RH buffering results for MCM-41$_{150}$ and MCM-41$_{180}$ – buffering application between $\varphi_{i,U}$ = 0.85 and $\varphi_{i,L}$ = 0.7

595

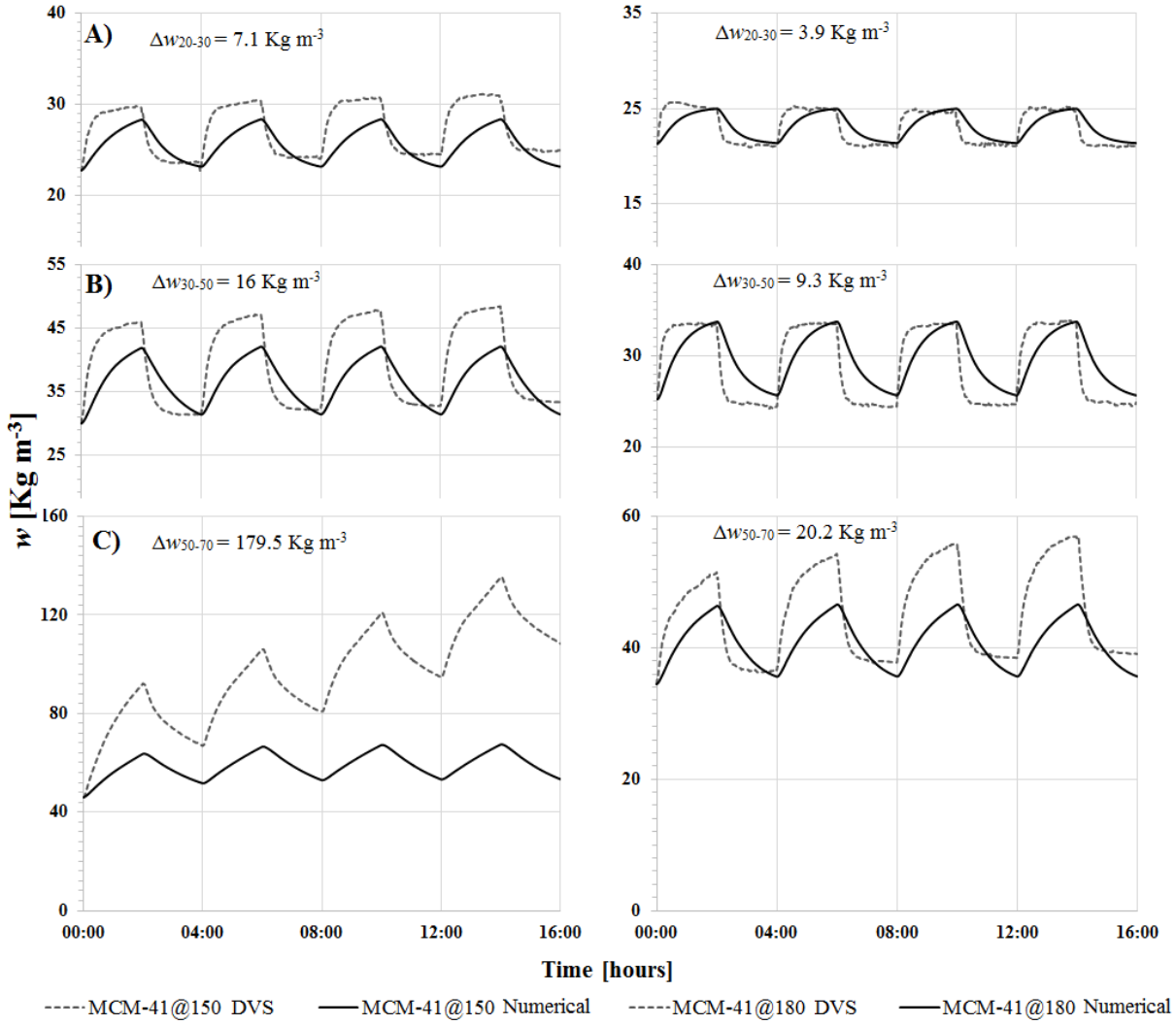

Figure 14 – Vapour sorption/ desorption kinetics in pre-defined RH limits, a) 20 - 30%, b) 30 - 50%, and c) 50 -70% – Comparison between numerical and experimental data

596

597

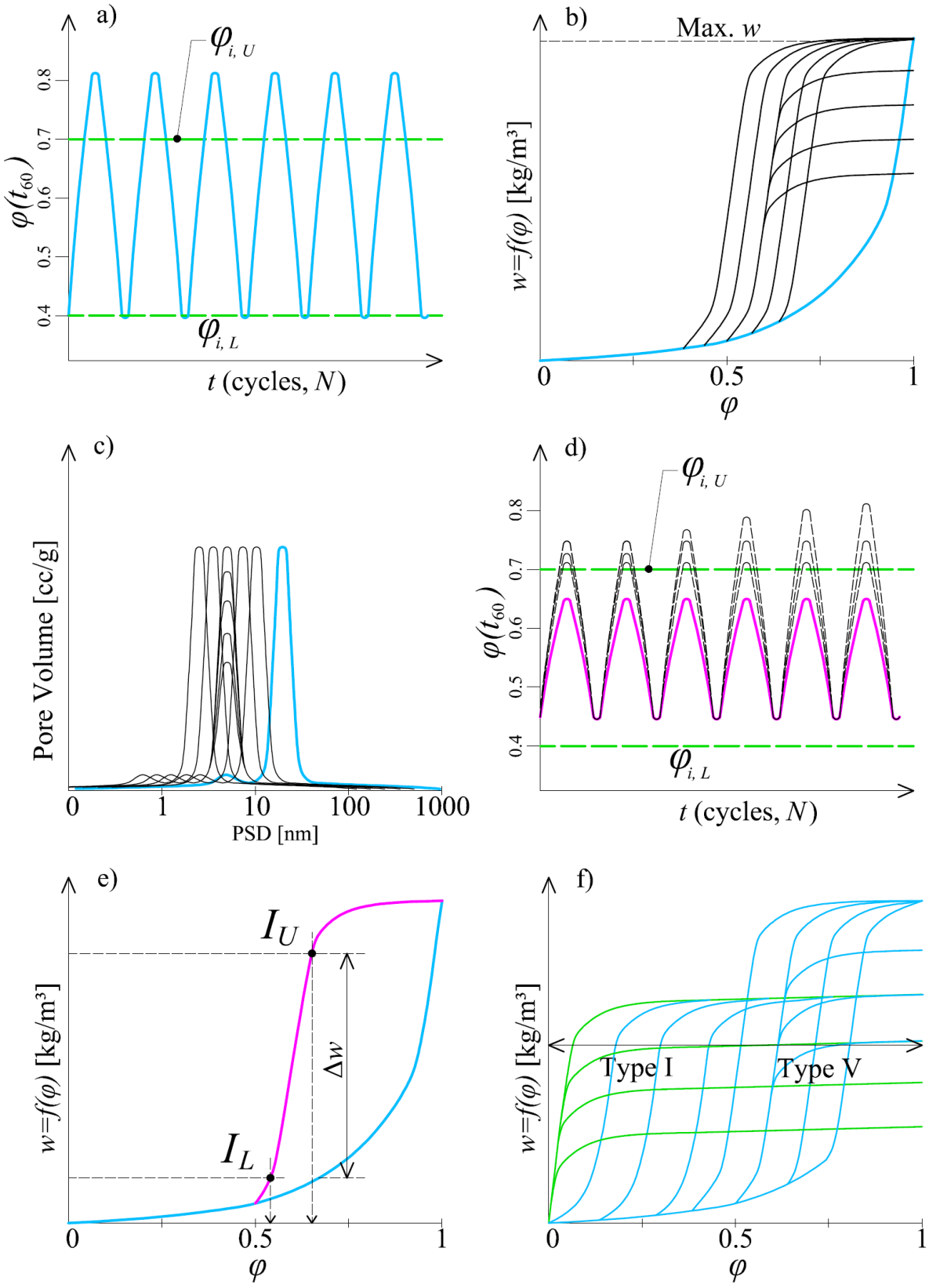

Figure 15 – Methodological illustration for the design process of an ideal isotherm

598

599

600

601 ## 8. Tables

Material	$\emptyset_{pore}$	ρ_{dry}	n	c_p	λ	w_{20}	w_{50}	w_{80}	w_f	A	μ
	nm	kg/m^3	m^3/m^3	J/kg·K	W/m·K	kg/m^3				Kg/m^2 s$^{0.5}$	---
MS 3.3 [A]	3.3	501	0.76	1011	0.05	12	79	247	346	2.112	4.54
MS 4.7 [A]	4.7	336	0.85	1866	0.05	8	33	105	363	0.561	7.13
MS 8.3 [A]	8.3	618	0.76	1691	0.05	5	86	295	865	0.550	10.52

Table 1 – Hygrothermal functional properties for mesoporous silicas – [A] Values taken from reference [20, 43]

602